Studies on GaAs-Based Light-Emitting Devices on Si Substrates for Optoelectronic Integrated Circuits

Contents

Chapter 1. Introduction

1.1 Background

A combination of GaAs-based compound semiconductors with highly developed Si has a great potential for creation of novel semiconductor materials incorporating photonic functions such as light emission and high speed operation into highly integrated Si-based electronic devices. Therefore, GaAs-based semiconductors on Si substrates (GaAs/Si) have attracted much interest as promising materials for future optoelectronic integrated circuits (OEICs)[1-8]. In the conventional Si-based devices, metallic wires and bonds have been used as electrical connections. On the other hand, for example, a Si-based ultra large scale integrated circuit (ULSI) chip with GaAs-based optical input/output (I/O) devices can hopefully promise the increased I/O speed and increased resistance to electromagnetic interference without time delays by optical chip-to-chip interconnects and communications. The communications can be carried out by high-speed optical links coupled through fibers or free-space propagation.

The merits and demerits of heteroepitaxy[9-13] and direct bonding (epitaxial lift-off)[12,14-27] are tabulated in Table I.I. For the realization of such a monolithic integration of GaAs and Si, many researches have been carried out by heteroepitaxy or direct bonding. In the latter, a homoepitaxially grown GaAs layer is transferred and bonded to Si substrate by adhesive metals and intermediate layers after detaching it from GaAs substrate. Direct bonding of GaAs/Si will provide high-quality GaAs film and possible uses of commercially processed Si chips. There are, however, some serious problems of troublesome fabrication, small area uniformity,

Table I.I. Merits and demerits of heteroepitaxy and direct bonding for GaAs on Si.

	Heteroepitaxy	Direct Bonding
Merits	Easy fabrication Large area uniformity as a substrate for other semiconductor devices for sollar cell applications Low cost	High-quality GaAs film on Si Possible uses of commercially processed Si chips
Demerits	Induced thermal stress High density dislocations	Troublesome fabrication Small area uniformity Induced thermal stress High resistance at the bonding interface

induced thermal stress and high resistance at the bonding interface. The heteroepitaxial growth of GaAs/Si has been actively studied over the past decade by molecular beam epitaxy (MBE) and metalorganic chemical vapor deposition (MOCVD). This heteroepitaxial growth technique has some attractive merits such as easy fabrication, large area uniformity and low cost. However, GaAs/Si material grown by heteroepitaxy suffers from three major problems:

(1) the anti-phase domain (APD) generation due to the polar (GaAs)-on-nonpolar (Si) system;

(2) the generation of high density of threading dislocations (>10^6 cm^{-2}) due to the ~4 % mismatch between the lattice constants of GaAs (0.5653 nm) and Si (0.5431 nm); and

(3) the large biaxial tensile stress (~10^9 dyn/cm^2) generated during cooling after the growth due to the difference in the thermal expansion coefficients of GaAs (6.4×10^{-6} /K) and Si (2.3×10^{-6} /K).

The relationship between lattice constants and thermal expansion coefficients at 300 K for various semiconductor materials is shown in Fig. 1.1. The first problem can lead to a low minority carrier lifetime[28] and poor morphology[29]. The latter two problems can contribute to the reduced minority carrier lifetimes[30] and the severe bowing of the GaAs/Si wafer which introduces microcracks[31-34] of the GaAs layer on Si. Thermally induced stress also enhances the migration of dislocations[35]. Considering the widespread applications of GaAs/Si, it is believed that the heteroepitaxy has more attractive advantages rather than the direct bonding. Therefore, for the growth of high-quality GaAs/Si, the above-

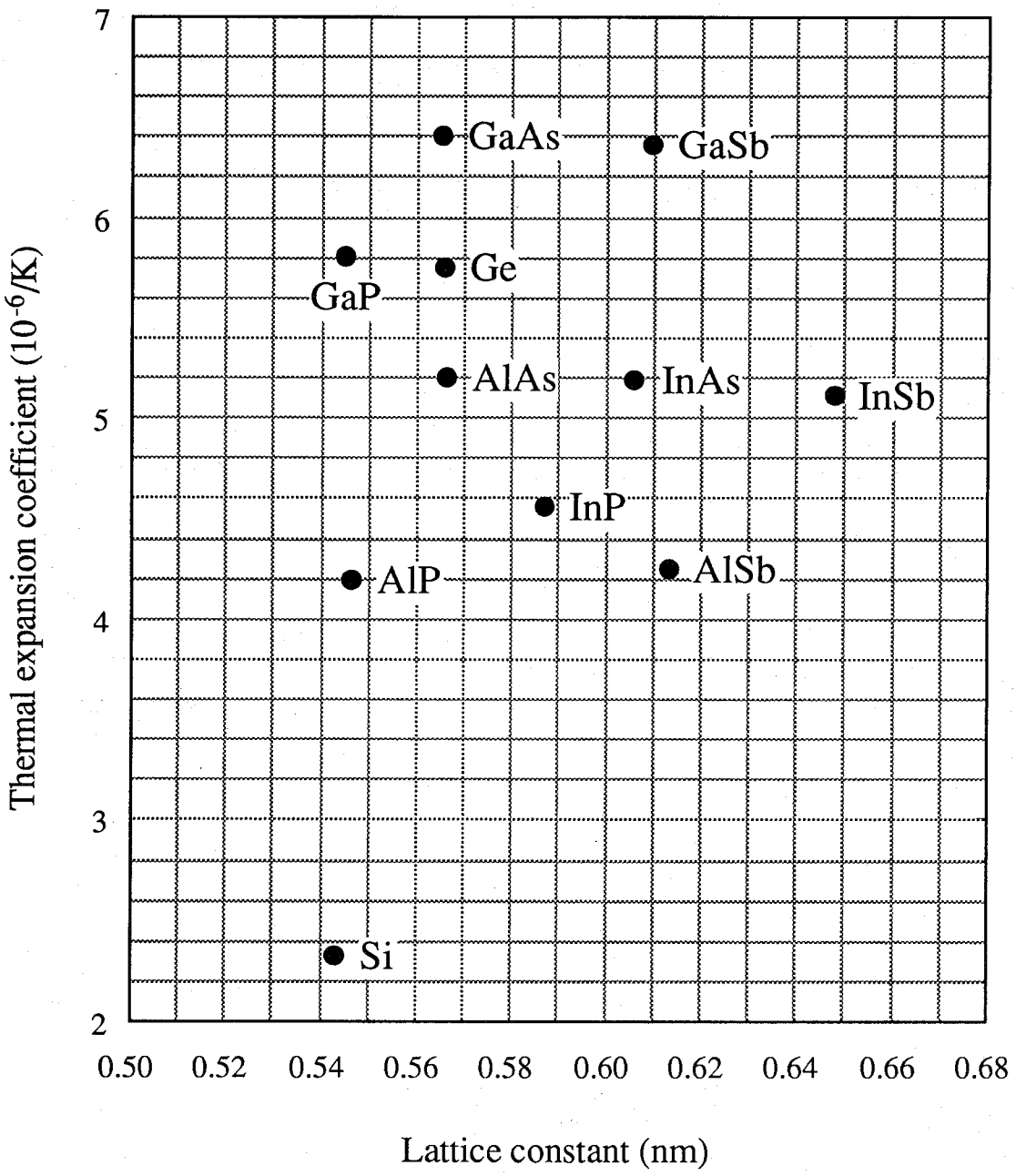

Fig. 1.1. Relationship between lattice constants and thermal expansion coefficients at 300 K for various semiconductor materials.

mentioned problems must be overcome.

1.2 Heteroepitaxial Growth of GaAs on Si

The above-mentioned first problem (APD generation) has been already solved by use of nominally (100)-oriented Si substrates with a slight misorientation between 2 and 4° towards the [011] direction[11,29,36-38]. This effect is accomplished through the formation of a (100) Si surface with a large density of double-atomic-layer steps on the Si surface as a result of the heat treatment of the misoriented Si substrate. Therefore, the Si substrates oriented 2° off (100) towards the [011] direction were used in this study. Although a single-domain GaAs layer was obtained by use of the misoriented Si substrate, the fundamental problems associated with the differences of lattice constant and thermal expansion coefficient still remain.

Most of the dislocations are confined at the GaAs/Si interface when grown by conventional MOCVD two-step growth technique[39] with an initial nucleation layer growth at relatively low temperature (~400 °C) and a subsequent growth at normal growth temperature. Growth at low temperature results in a mode approaching two-dimensional GaAs nucleation layer growth[40]. The number of threading dislocations can be decreased by inserting strained-layer superlattices (SLSs)[11] such as InGaAs/GaAs[41,42] and GaAsP/GaAs[9,43]. Nozawa and co-workers[44] have reported that the etch pit density (EPD) was drastically reduced to 7×10^4 cm^{-2} by a combination of InGaAs/GaAs SLSs inserted into GaAs layers on Si grown by migration enhanced epitaxy (MEE) at 300 °C. Recently, other new approaches such as $(GaAs)_m(GaP)_n$ strained short-period superlattices (SSPSs)[45], ZnSe[46,47] and GaSe[48] buffer layers, thin

Si intermediate layer[13,49,50] and so on, have been proposed. In addition, in-situ[41,42,51,52] and ex-situ[11,53-55] thermal annealings are also effective in reducing the dislocation density due to the increase of dislocation velocity and interaction. The growth on the pre-patterned Si substrates is also useful for reducing the dislocation density[12,55-62]. For example, Ismail et al.[57] have demonstrated low dislocation density of ~10^5 cm^{-2} in the GaAs layer grown on a sawtooth patterned Si substrate. This effect seems to be caused by the presence of a thin SiO_2 layer at the GaAs/Si interface, resulting in the relaxation of lattice mismatch strain.

The reduction of thermal stress has been demonstrated by uses of selective-area growth[63-66] and post-growth patterning[42,54,67,68]. The residual stress and the defect density in the GaAs/Si decrease with reductions of the growth area. This is due to the fact that the stress near the edge is released, because the edge facet is free to move[67]. Another approach to reduce the thermal stress is proposed by using a selective etching AlGaAs release layer to undercut GaAs mesa structures[12,43,69-76]. The completely undercut mesas are restrained in their original positions by photoresist positioners, and the residual stress is completely removed by this mesa release and deposition (MRD) technique[69-71]. Sakai et al.[43,72-76] have proposed the undercut GaAs/Si (UCGAS) where only part of the GaAs layer is undercut. This UCGAS is useful for both the reduction of dislocation density and thermal stress after post-growth annealing. This effect is believed to be caused by the absence of the GaAs/Si interface which acts as a source for dislocation supply.

In spite of these efforts, the threading dislocation density below 10^4 cm^{-2}, which is allowed to use for practical devices

(especially light-emitting devices), has not been realized yet.

1.3 Device Applications: Light-Emitting Devices on Si

In spite of the above-mentioned problems, numerous GaAs-based electrical and optical devices, including field-effect transistors (FETs)[77], high-electron-mobility transistors (HEMTs)[78,79], modulators[80], waveguides[81], photodetectors[82], solar sells[10,83], LEDs[74,76] and lasers[84-91], have been fabricated on Si substrates by heteroepitaxy.

The characteristics of GaAs/Si electrical devices have been improved to the same level as that of GaAs/GaAs, because the majority carriers are hardly influenced by the dislocation density.

On the other hand, the characteristics of the light-emitting devices operated by minority carriers are easily affected by dislocations[10]. However, most of the interest has been focused on the realization of reliable GaAs-based LEDs and lasers on Si because of needs for optical interconnects in future OEICs. In 1984, Windhorn et al.[84] were the first to report the pulsed operation at 77 K for an AlGaAs/GaAs double-heterostructure (DH) laser on Si grown by MBE (threshold current density: J_{th}=~10 kA/cm^2). They also reported that MBE-grown AlGaAs/GaAs single quantum well (SQW) laser was operated under pulsed condition at room-temperature in 1986 (J_{th}=~4 kA/cm^2)[85]. In the same year, the first AlGaAs/GaAs DH laser on Si grown by MOCVD was reported by Sakai et al.[86]. This laser was operated under pulsed condition at room-temperature (J_{th}=~1.5 kA/cm^2). In 1987, Deppe et al.[87] succeeded in the first room-temperature continuous-wave (cw) operation for an AlGaAs/GaAs SQW laser grown by MOCVD on MBE-grown GaAs-coated Si substrate (J_{th}=~2 kA/cm^2). This laser was operated for ~4.5 h under cw

condition at room-temperature. The cw lifetime was increased to ~16 h by use of microcracks for an AlGaAs/GaAs SQW laser on Si[33] in 1988. In 1989, room-temperature cw operation for an AlGaAs/GaAs laser on Si grown by only MOCVD was achieved by Egawa et al.[88]. In 1990, Deppe et al.[89,90] reported the first demonstration of vertical-cavity surface-emitting laser (VCSEL) on Si. The cw lifetime of ~56.5 h was reported by Choi et al.[91] for an AlGaAs/InGaAs SQW laser on Si in 1991. For the LEDs on Si, Wada et al.[74] reported the lifetime over 2500 h for an undercut AlGaAs/GaAs LED under direct current (dc) condition at room-temperature in 1992. Furthermore, in 1993, an AlGaAs/GaAs SQW laser on a sawtooth Si substrate was operated under room-temperature cw condition for ~100 h[12]. The summary of recent advances in the GaAs-based light-emitting devices on Si is shown in Table I.II. In this table, those of the InP-based light-emitting devices on Si[92-95] are also shown as references. The InP-based lasers on Si have advantages of reliability over the GaAs-based lasers on Si, because the dark-line defect (DLD) growth velocity in the active layer of the InP-based lasers is about two order lower than that of the GaAs-based lasers[96,97]. Therefore, a long-wavelength (1.5 μm) InGaAsP/InGaAs multi quantum well (MQW) laser on Si[94,98] has exhibited no degradation after more than 8000 h under cw condition at room-temperature, despite the high dislocation density of ~10^7 cm^{-2}.

1.4 Purpose and Organization of Dissertation

GaAs-based light-emitting devices on Si suffer from rapid degradation, and reliable GaAs-based devices on Si for practical use have not been realized yet. The understanding of the rapid degradation mechanisms is very important in order to obtain highly

Table I.II. Summary of recent advances in GaAs- and InP-based light-emitting devices on Si.

Year	GaAs-based light-emittimg devices	InP-based light-emitting devices
1995		InP/InGaAsP DH laser on Si (MOCVD+VME) lifetime > 800 h (300 K, CW) (λ= 1.3 μm) [NTT]
1993	AlGaAs/GaAs SQW laser on sawtooth Si (MOCVD) lifetime ~100 h (300 K, CW) [IMEC]	
1992	Undercut (UC) AlGaAs/GaAs LED on Si (MOCVD) lifetime > 2500 h (300 K, DC) [Tokushima Univ.] Stress-free mesa release and deposition (MRD) AlGaAs/GaAs DH laser on Si (MOCVD) [MIT]	InGaAsP/InGaAs MQW laser on Si (MOCVD+VME) lifetime > 8000 h (300 K, CW) (λ= 1.5 μm) [NTT] ※VME ; vapor mixing epitaxy
1991	AlGaAs/GaAs SQW laser on Si with microcracks (MBE+MOCVD) lifetime ~500 h (200 K, CW) [Illinois Univ.] AlGaAs/InGaAs SQW laser on Si (MOCVD) lifetime ~56.5 h (300 K, CW) [MIT] AlGaAs/GaAs SQW laser on Si using selective growth (MOCVD) lifetime ~10 h (300 K, CW) [MIT]	
1990	AlGaAs/GaAs VCSEL on Si (MBE) I_{th} = 125 mA (300 K, Pulsed) [AT&T]	
1989	AlGaAs/GaAs SQW laser on Si (MOCVD) (300 K, CW) [NIT]	
1988	AlGaAs/GaAs SQW laser on Si with microcracks (MBE+MOCVD) lifetime ~16 h (300 K, CW) [Illinois Univ.]	InP/InGaAsP DH laser on Si (MOCVD) lifetime > 5 h (300 K, CW) (λ= 1.3 μm) [Thomson-CSF] InP/InGaAsP LED on Si (MOCVD) lifetime ~24 h (300 K, DC) (λ= 1.15 μm) [Thomson-CSF]
1987	AlGaAs/GaAs SQW laser on Si (MBE+MOCVD) lifetime ~4 .5 h (300 K, CW) [Illinois Univ.] AlGaAs/GaAs SQW laser on Si (MOCVD) (375 K, Pulsed) (< 160 K, CW) [AT&T]	
1986	AlGaAs/GaAs DH laser on Si (MOCVD) (290 K, Pulsed) [NIT] AlGaAs/GaAs SQW laser on Si (MBE) (300 K, Pulsed) [MIT]	
1984	AlGaAs/GaAs DH laser on Si (MBE) (77 K, Pulsed) [MIT]	

reliable GaAs-based LEDs and lasers on Si. Novel approaches must be proposed for suppression of the degradation.

The dissertation is composed of six chapters, and each of them is summarized below.

In chapter 2, degradation mechanisms related to DLDs for AlGaAs/GaAs quantum well lasers on Si are described. Using electroluminescence (EL) topography, the detailed observation of rapid degradation of the lasers on Si is carried out under cw aging operation at room-temperature. The generation and rapid expansion of the <100> DLDs is clearly observed, resulting in the deterioration of lasing characteristic parameters such as internal differential quantum efficiency, differential gain coefficient and internal loss. Additionally, it is also shown that the DLD growth velocity depends on the injected current density.

In chapter 3, increased lifetimes of strained AlGaAs/InGaAs quantum well lasers on Si with InGaAs intermediate layers (InGaAs ILs) are presented. The increased lifetimes are achieved by both introducing InGaAs ILs and replacing the conventional GaAs active layers with the InGaAs layers. EL topography shows the suppression of <100> DLD growth velocity with the increase of In content in the InGaAs active layer. Furthermore, a remarkable improvement in reliability of a post-growth annealed AlGaAs/$In_{0.07}Ga_{0.93}As$ laser on Si with InGaAs IL is also given.

In chapter 4, improved characteristics of AlGaAs/GaAs light-emitting devices on Si by reducing the active regions are described. The structures of vertically-stacked quasi GaAs quantum wires grown on a V-grooved GaAs/Si substrate are confirmed by a high-resolution scanning electron microscopy (SEM). The extremely low-threshold current AlGaAs/GaAs quantum wire-like laser on Si is also demonstrated. Furthermore, an AlGaAs/GaAs LED on Si with self-

formed GaAs islands active region is presented. The shape and size of GaAs islands formed by droplet-epitaxy are characterized by an atomic force microscopy (AFM). The reliability of this LED is also demonstrated.

In chapter 5, the fabrication of AlGaAs/GaAs VCSELs on Si is presented. Room-temperature pulsed operation for a VCSEL on Si with bottom mirror of a 20-pair of AlAs/GaAs quarter-wave multilayer distributed Bragg reflector (DBR), top mirror of nonalloyed AuZn/Au and a SQW active layer is described. Furthermore, it is demonstrated that a VCSEL on Si with bottom mirror of a 23-pair of AlAs/$Al_{0.1}Ga_{0.9}As$ DBR, top mirror of transparent Au and ten quantum wells succeeded in the cw operation at low-temperature up to 150 K.

Chapter 6 is the summary of this dissertation.

References

1) H. K. Choi, J. P. Mattia, G. W. Turner and B.-Y. Tsaur, IEEE Electron Device Lett., **9**, 512 (1988).

2) H. Shichijo, R. Matyi, A. H. Taddiken and Y.-C. Kao, IEEE Trans. Electron Devices, **37**, 548 (1990).

3) T. Egawa, T. Jimbo and M. Umeno, IEEE Photon. Technol. Lett., **4**, 612 (1992).

4) T. Egawa, T. Jimbo and M. Umeno, IEICE Trans. Electron., **E76-C**, 106 (1993).

5) G. N. Nasserbakht, J. W. Adkisson, B. A. Wooley, J. S. Harris and T. I. Kamins, IEEE J. Solid-State Circuits, **28**, 622 (1993).

6) I. Hayashi, Jpn. J. Appl. Phys., **32**, 266 (1993).

7) I. Hayashi, Optoelectron. Devices Technol., **9**, 468 (1994).

8) K. W. Goossen, J. A. Walker, L. A. D'Asaro, S. P. Hui, B. Tseng, R. Leibenguth, D. Kossives, D. D. Bacon, D. Dahringer, L. M. F. Chirovsky, A. L. Lentine and D. A. B. Miller, IEEE Photon. Technol. Lett., **7**, 360 (1995).

9) R. D. Dupuis and C. J. Pinzone, J. Cryst. Growth, **93**, 434 (1988).

10) M. Yamaguchi and S. Kondo, *Mat. Res. Soc. Symp. Proc.*, **145**, 279 (1989).

11) S. F. Fang, K. Adomi, S. Iyer, H. Morkoc, H. Zabel, C. Choi and N. Otsuka, J. Appl. Phys., **68**, R31 (1990).

12) J. De Boeck and G. Borghs, J. Cryst. Growth, **127**, 85 (1993).

13) M. Tamura, Optoelectron. Devices Technol., **9**, 93 (1994).

14) E. Yablonovitch, E. Kapon, T. J. Gmitter, C. P. Yun and R. Bhat, IEEE Photon. Technol. Lett., **1**, 41 (1989).

15) J. F. Klem, E. D. Jones, D. R. Myers and J. A. Lott, J. Appl. Phys., **66**, 459 (1989).

16) I. Pollentier, P. Demeester, A. Ackaert, L. Buydens, P. V. Daele and R. Baets, Electron. Lett., **26**, 193 (1990).

17) G. W. Yoffe and J. M. Dell, Electron. Lett., **27**, 557 (1991).

18) I. Pollentier, L. Buydens, P. Van Daele and P. Demeester, IEEE Photon. Technol. Lett., **3**, 115 (1991).

19) A. Ersen, I. Schnitzer, E. Yablonovitch and T. Gmitter, Solid-State Electron., **36**, 1731 (1993).

20) B. D. Dingle, M. B. Spitzer, R. W. McClelland, J. C. C. Fan and P. M. Zavracky, Appl. Phys. Lett., **62**, 2760 (1993).

21) K. W. Goossen, J. E. Cunningham and W. Y. Jan, IEEE Photon. Technol. Lett., **5**, 776 (1993).

22) Y. H. Lo, R. Bhat, D. M. Hwang, C. Chua and C.-H. Lin, Appl. Phys. Lett., **62**, 1038 (1993).

23) H. Fathollahnejab, D. L. Mathine, R. Droopad, G. N. Maracas and S. Daryanani, Electron. Lett., **30**, 1235 (1994).

24) H.-J. J. Yeh and J. S. Smith, Appl. Phys. Lett., **64**, 1466 (1994).

25) H.-J. J. Yeh and J. S. Smith, IEEE Photon. Technol. Lett., **6**, 706 (1994).

26) K. Zaharaman, J.-C. Guillaume, G. Nataf, B. Beaumont, M. Leroux and P. Gibart, Jpn. J. Appl. Phys., **33**, 5807 (1994).

27) J. K. Tu, J. J. Talghader, M. A. Hadley and J. S. Smith, Electron. Lett., **31**, 1448 (1995).

28) K. Nauka, G. A. Reid and Z. L.-Weber, Appl. Phys. Lett., **56**, 376 (1990).

29) H. Noge, H. Kano, M. Hashimoto and I. Igarashi, J. Appl. Phys., **64**, 2246 (1988).

30) R. K. Ahrenkiel, M. M. Al-Jassim, D. J. Dunlavy, K. M. Jones, S. M. Vernon, S. P. Tobin and V. E. Haven, Appl. Phys. Lett., **53**, 222 (1988).

31) R. W. Kaliski, N. Holonyak, Jr., K. C. Hsieh, D. W. Nam, J. W. Lee, H. Shichijo, R. D. Burnham, J. E. Epler and H. F. Chung, Appl. Phys. Lett., **50**, 836 (1987).

32) B. G. Yacobi, S. Zemon, P. Norris, C. Jagannath and P. Sheldon, Appl. Phys. Lett., **51**, 2236 (1987).

33) D. G. Deppe, D. C. Hall, N. Holonyak, Jr., R. J. Matyi, H. Shichijo and J. E. Epler, Appl. Phys. Lett., **53**, 874 (1988).

34) N. Hayafuji, H. Kizuki, M. Miyashita, K. Kadoiwa, T. Nishimura, N. Ogasawara, H. Kumabe, T. Murotani and A. Tada, Jpn. J. Appl. Phys., **30**, 459 (1991).

35) M. Tachikawa and H. Mori, Appl. Phys. Lett., **56**, 2225 (1990).

36) T. Ueda, S. Nishi, Y. Kawarada, M. Akiyama and K. Kaminishi, Jpn. J. Appl. Phys., **25**, L789 (1986).

37) R. Fischer, D. Neuman, H. Zabel, H. Morkoc, C. Choi and N. Otsuka, Appl. Phys. Lett., **48**, 1223 (1986).

38) S. N. G. Chu, S. Nakahara, S. J. Pearton, T. Boone and S. M. Vernon, J. Appl. Phys., **64**, 2981 (1988).

39) M. Akiyama, Y. Kawarada and K. Kaminishi, Jpn. J. Appl. Phys., **23**, L843 (1984).

40) D. K. Biegelsen, F. A. Ponce, A. J. Smith and J. C. Tramontana, *Mat. Res. Soc. Symp. Proc.*, **67**, 45 (1986).

41) H. Okamoto, Y. Watanabe, Y. Kadota and Y. Ohmachi, Jpn. J. Appl. Phys., **26**, L1950 (1987).

42) T. Egawa, Y. Hasegawa, T. Jimbo and M. Umeno, Jpn. J. Appl. Phys., **31**, 791 (1992).

43) N. Wada, S. Sakai and M. Fukui, Jpn. J. Appl. Phys., **33**, 976 (1994).

44) K. Nozawa and Y. Horikoshi, Jpn. J. Appl. Phys., **30**, L668 (1991).

45) T. Kawai, H. Yonezu, Y. Ogasawara, D. Saito and K. Pak, Appl.

Phys. Lett., **63**, 2067 (1993).

46) M. K. Lee, R. H. Horng, D. S. Wuu and P. C. Chen, Appl. Phys. Lett., **59**, 207 (1991).

47) R. D. Bringans, D. K. Biegelsen, L.-E. Swartz, F. A. Ponce and J. C. Tramontana, Appl. Phys. Lett., **61**, 195 (1992).

48) J. E. Palmer, T. Saitoh, T. Yodo and M. Tamura, Jpn. J. Appl. Phys., **32**, L1126 (1993).

49) A. Hashimoto, N. Sugiyama and M. Tamura, Jpn. J. Appl. Phys., **30**, L447 (1991).

50) T. S. Rao, K. Nozawa and Y. Horikoshi, Appl. Phys. Lett., **62**, 154 (1993).

51) H. L. Tsai and J. W. Lee, Appl. Phys. Lett., **51**, 130 (1987).

52) M. Yamaguchi, A. Yamamoto, M. Tachikawa, Y. Itoh and M. Sugo, Appl. Phys. Lett., **53**, 2293 (1988).

53) R. W. Kaliski, C. R. Ito, D. G. Mclntyre, M. Feng, H. B. Kim, R. Bean, K. Zanio and K. C. Hsieh, J. Appl. Phys., **64**, 1196 (1988).

54) N. Chand and S. N. G. Chu, Appl. Phys. Lett., **58**, 74 (1991).

55) M. Tamura, A. Hashimoto, J. Kasai and A. Nishida, J. Cryst. Growth, **147**, 264 (1995).

56) A. Hashimoto, T. Fukunaga and N. Watanabe, Appl. Phys. Lett., **54**, 998 (1989).

57) K. Ismail, F. Legoues, N. H. Karam, J. Carter and H. I. Smith, Appl. Phys. Lett., **59**, 2418 (1991).

58) K.-R. Sprung, K. Wilke, G. Heymann, J. Varrio and M. Pessa, Appl. Phys. Lett., **62**, 2711 (1993).

59) R. Murray, C. Roberts, K. Woodbridge, P. Barnes, G. Parry and C. Norman, Appl. Phys. Lett., **62**, 2929 (1993).

60) J. G. Zhu, M. M. Al-Jassim, N. H. Karam and K. M. Jones, *Mat. Res. Soc. Symp. Proc.*, **281**, 327 (1993).

61) A. Krost, R. F. Schnabel, F. Heinrichsdorff, U. Rossow, D. Bimberg and H. Cerva, J. Cryst. Growth, **145**, 314 (1994).

62) J. Knall, L. T. Romano, D. K. Biegelsen, R. D. Bringans, H. C. Chui, J. S. Harris, Jr., D. W. Treat and D. P. Bour, J. Appl. Phys., **76**, 2697 (1994).

63) M. Yamaguchi, M. Tachikawa, M. Sugo, S. Kondo and Y. Itoh, Appl. Phys. Lett., **56**, 27 (1990).

64) H. P. Lee, X. Liu and S. Wang, Appl. Phys. Lett., **56**, 1014 (1990).

65) H. P. Lee, X. Liu and S. Wang, J. Vac. Sci. Technol., B **8**, 343 (1990).

66) Y. Kobayashi, T. Egawa, T. Jimbo and M. Umeno, Jpn. J. Appl. Phys., **30**, L1781 (1991).

67) J. P. van der Ziel, N. Chand and J. S. Weiner, J. Appl. Phys., **66**, 1195 (1989).

68) J. P. van der Ziel and N. Chand, J. Appl. Phys., **68**, 2731 (1990).

69) J. De Boeck, C. Van Hoof, K. Deneffe, R. P. Mertens and G. Borghs, Appl. Phys. Lett., **59**, 1179 (1991).

70) G. F. Burns and C. G. Fonstad, Appl. Phys. Lett., **61**, 2199 (1992).

71) G. F. Burns and C. G. Fonstad, IEEE Photon. Technol. Lett., **4**, 18 (1992).

72) S. Sakai, K. Kawasaki and N. Wada, Jpn. J. Appl. Phys., **29**, L853 (1990).

73) N. Wada, K. Iwabu, S. Sakai and M. Fukui, Appl. Phys. Lett., **60**, 1354 (1992).

74) N. Wada, S. Yoshimi, M. Shigekane, S. Sakai, Y. Shintani and M. Fukui, *Extended Abstracts of the 1992 Int. Conf. Solid State Devices and Materials* (Tsukuba, 1992) p. 650.

75) N. Wada, S. Sakai and M. Fukui, Jpn. J. Appl. Phys., **33**, 864 (1994).

76) N. Wada, S. Sakai, S. Yoshimi, Y. Shintani and M. Fukui, Jpn. J. Appl. Phys., **33**, 1268 (1994).

77) T. Egawa, S. Nozaki, T. Soga, T. Jimbo and M. Umeno, Appl. Phys. Lett., **58**, 1265 (1991).

78) T. Aigo, A. Jono, A. Tachikawa, R. Hiratsuka and A. Moritani, Appl. Phys. Lett., **64**, 3127 (1994).

79) T. Ohori, H. Suehiro, K. Kasai and J. Komeno, Jpn. J. Appl. Phys., **33**, 4499 (1994).

80) K. W. Goossen, G. D. Boyd, J. E. Cunningham, W. Y. Jan, D. A. B. Miller, D. S. Chemla and R. M. Lum, IEEE Photon. Technol. Lett., **1**, 304 (1989).

81) T. Yuasa, Y. Nagashima, T. Murase, T. Jimbo and M. Umeno, Jpn. J. Appl. Phys., **32**, L1055 (1993).

82) J. Paslaski, H. Z. Chen, H. Morkoc and A. Yariv, Appl. Phys. Lett., **52**, 1410 (1988).

83) M. Yang, T. Soga, T. Jimbo and M. Umeno, Jpn. J. Appl. Phys., **33**, 6605 (1994).

84) T. H. Windhorn, G. M. Metze, B.-Y. Tsaur and J. C. C. Fan, Appl. Phys. Lett., **45**, 309 (1984).

85) T. H. Windhorn, G. W. Turner and G. M. Metze, *Mat. Res. Soc. Symp. Proc.*, **67**, 157 (1986).

86) S. Sakai, T. Soga, M. Takeyasu and M. Umeno, Appl. Phys. Lett., **48**, 413 (1986).

87) D. G. Deppe, D. W. Nam, N. Holonyak, Jr., K. C. Hsieh, R. J. Matyi, H. Shichijo, J. E. Epler and H. F. Chung, Appl. Phys. Lett., **51**, 1271 (1987).

88) T. Egawa, H. Tada, Y. Kobayashi, T. Soga, T. Jimbo and M. Umeno, Appl. Phys. Lett., **57**, 1179 (1990).

89) D. G. Deppe, N. Chand, J. P. van der Ziel and G. J. Zydzik, Appl. Phys. Lett., **56**, 740 (1990).

90) D. Cherns, D. Loretto, N. Chand, D. Bahnck and J. M. Gibson, Philos. Mag., A **63**, 1335 (1991).

91) H. K. Choi, C. A. Wang and N. H. Karam, Appl. Phys. Lett., **59**, 2634 (1991).

92) M. Razeghi, R. Blondeau, M. Defour, F. Omnes, P. Maurel and F. Brillouet, Appl. Phys. Lett., **53**, 854 (1988).

93) M. Razeghi, M. Defour, R. Blondeau, F. Omnes, P. Maurel, O. Acher, F. Brillouet, J. C. C. Fan and J. Salerno, Appl. Phys. Lett., **53**, 2389 (1988).

94) M. Sugo, H. Mori, Y. Itoh and Y. Sakai, *Extended Abstracts of the 1992 Int. Conf. Solid State Devices and Materials* (Tsukuba, 1992) p. 656.

95) T. Yamada, M. Tachikawa, T. Sasaki, H. Mori, Y. Kadota and M. Yamamoto, Electron. Lett., **31**, 455 (1995).

96) M. Fukuda, K. Wakita and G. Iwane, J. Appl. Phys., **54**, 1246 (1983).

97) O. Ueda, J. Electrochem. Soc., **135**, 11C (1988).

98) M. Sugo, H. Mori, Y. Sakai and Y. Itoh, Appl. Phys. Lett., **60**, 472 (1992).

Chapter 2. Degradation Mechanisms of AlGaAs/GaAs Quantum Well Lasers on Si Substrates

2.1 Introduction

Observation of the degradation of GaAs-based lasers on Si is very important for understanding of the rapid degradation mechanism and development of long-life reliable lasers. Van der Ziel and co-workers[1,2] have reported that growth of nonradiative dark regions including DLDs was observed in an AlGaAs/GaAs SQW laser on Si using pulsed current excitation. Martins et al.[3] have reported that the initial degradation of the AlGaAs/GaAs SQW laser on Si occurred in the vicinity of the p-n junction. Recently, Egawa et al.[4] have observed optical and electrical degradation of the AlGaAs/GaAs SQW laser on Si. However, rapid degradation mechanisms related to DLDs under cw aging operation have not been clarified.

In this chapter, the influences of DLDs on lasing characteristics and the dependence of DLD growth velocity on the injected current density for the AlGaAs/GaAs quantum well laser on Si are described. This chapter is organized as follows: In section 2.2, epitaxial growth and fabrication process of the AlGaAs/GaAs quantum well laser on Si are described. The influences of DLDs on lasing characteristics under cw aging operation are presented in section 2.3. In section 2.4, the dependence of <100> and <110> DLD growth velocities on the injected current density under direct current (dc) operation is described. This chapter is concluded in section 2.5.

2.2 Epitaxial Growth and Fabrication Process

The samples used in this study were grown on n^+-Si substrates (Sb-doped, 0.02 Ω·cm) oriented 2° off (100) towards the [011] direction by MOCVD, using an rf-heated horizontal reactor operated at atmospheric pressure. Trimethylgallium (TMG) and trimethylaluminum (TMA) were used as group-III sources, and arsine (AsH_3) was used as a group-V source. Hydrogen selenide (H_2Se) and diethylzinc (DEZ) were used as n- and p-dopants, respectively. The carrier gas was hydrogen (H_2). The substrates were rinsed in organic solvents and then cleaned in solutions of H_2SO_4:H_2O_2 (4:1 by volume) and HF:H_2O (1:1 by volume). Prior to the growth, the substrates were heated in H_2 atmosphere at 1000 °C for 10 min in order to remove the native oxide from the substrate surface. The growth temperature was 750 °C except for the initial GaAs nucleation layer which was grown on Si at 400 °C in the two-step growth technique. An initial 10-nm-thick undoped GaAs nucleation layer and a 2.1-μm-thick n^+-GaAs buffer layer (Se-doped, 2×10^{18} cm^{-3}) were grown. During growth of the n^+-GaAs layer, the substrate temperature was cycled five times from 350 to 850 °C in an AsH_3 atmosphere. This thermal cycle annealing is effective in reducing the threading dislocations in the active layers of the lasers[5,6]. Figure 2.1 shows a schematic cross-section of an AlGaAs/GaAs triple quantum well (TQW) laser on Si. The laser structure comprised a 1.0-μm-thick n-$Al_{0.7}Ga_{0.3}As$ lower cladding layer (Se-doped, 1×10^{18} cm^{-3}), a 60-nm-thick undoped $Al_{0.3}Ga_{0.7}As$ lower optical confining layer, three 9-nm-thick undoped GaAs quantum wells separated by 5.5-nm-thick undoped $Al_{0.3}Ga_{0.7}As$ barrier layers, a 60-nm-thick undoped $Al_{0.3}Ga_{0.7}As$ upper optical confining layer, a 1.0-μm-thick p-$Al_{0.7}Ga_{0.3}As$ upper cladding layer (Zn-doped, 1×10^{18} cm^{-3}) and an 80-nm-thick p^+-GaAs contact layer (Zn-doped, 1×10^{19} cm^{-3}). After the growth, laser devices were fabricated as follows. A 0.1-μm-

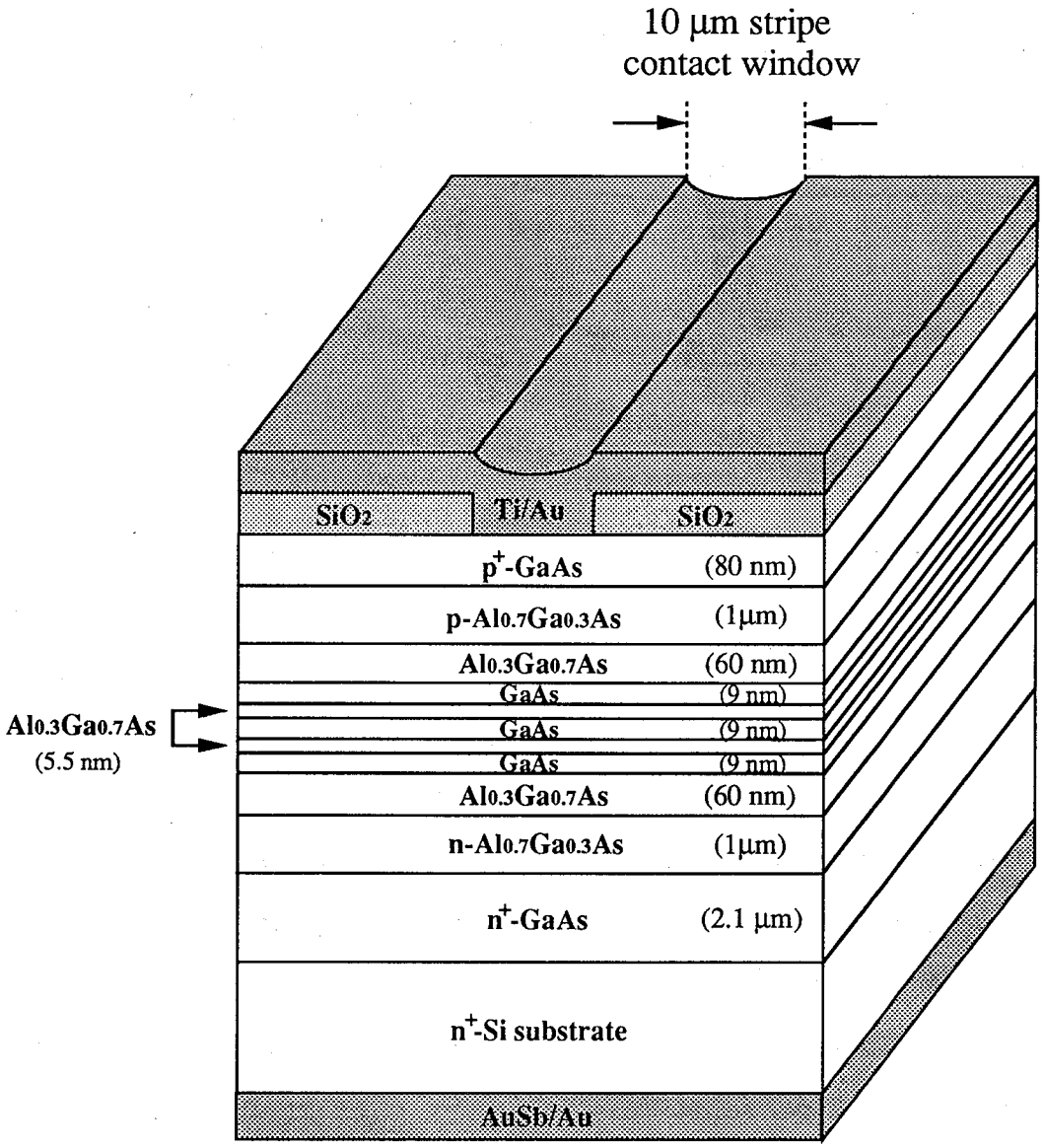

Fig. 2.1. Schematic cross-section of AlGaAs/GaAs TQW laser on Si.

thick SiO_2 insulating layer was deposited on the p^+-GaAs contact layer and 10-μm-wide stripe contact windows were opened with a 300 μm pitch along the <110> direction by chemical etching of SiO_2. Then, 50-nm-thick Ti/150-nm-thick Au were evaporated on the p^+-GaAs layer as the p-side electrode. After thinning the n^+-Si substrate to a thickness of 100 μm, 50-nm-thick AuSb/150-nm-thick Au were evaporated on the Si substrate as the n-side electrode. The contacts were annealed in a N_2 atmosphere at 380 °C for 30 s to reduce the series resistance. The samples were cleaved into chips and mounted on In-soldered Cu heatsinks in the p-side-up configuration. In order to observe the electroluminescence (EL) topograph of the active region with a Si vidicon TV camera (Hamamatsu C2741-03), part of the p-side electrode of the lasers was thinned by chemical etching in a solution of KI : I_2 : H_2O (113 g : 65 g : 100 cm^3)[7].

The AlGaAs/GaAs TQW lasers on Si with 120-800 μm cavity length were prepared. The cw aging test was carried out at a constant output power of 1 mW/facet under automatic power control (APC) operation at a heatsink and ambient temperature of 20 °C. The degree of degradation was studied through the change of the increase ratio of cw driving current (ΔI), lasing characteristic parameters such as internal differential quantum efficiency (η_i), internal loss (α_i) and differential gain coefficient (β), and EL topograph of the active region[8]. ΔI was determined using

$$\Delta I = (I - I_0) / I_0 \times 100, \qquad (2.1)$$

where I and I_0 are driving current and its initial value, respectively.

2.3 Influences of DLDs on Lasing Characteristics

All AlGaAs/GaAs TQW lasers on Si degraded within a few minutes. No relationship between the lifetime and the cavity length of the lasers was observed in this experiment. Figure 2.2 shows the log-log relationship between the increase ratio of driving current (ΔI) and aging time for the lasers on Si. The driving current increases almost linearly with operating time at the initial slow degradation stage of ΔI < 60-80 %. However, at the subsequent rapid degradation stage of ΔI > 60-80 %, the driving current increases approximately as the eighth power of operating time. These results indicate that the degradation mechanisms differ in the initial slow degradation stage and the subsequent rapid one. In order to investigate this difference, the EL topographs of the laser on Si were observed at each degradation stage. Typical EL topographs at each degradation stage of ΔI = 0, 40, 100, 200 % are shown in Fig. 2.3. At the initial slow degradation stage of ΔI = 40 %, generation of a few <100> DLDs was observed. Subsequently, expansion of <100> DLDs was clearly observed at the rapid degradation stages of ΔI = 100, 200 %. Detailed observations of DLD growth are described in section 2.4.

In order to observe the change of lasing characteristics for the lasers on Si, light-versus-current (L-I) characteristics were measured at 20 °C at each degradation stage by interrupting the aging test. Figure 2.4 shows the typical L-I characteristics of the 425-μm-long laser on Si under the pulsed condition at each degradation stage. Current pulses 0.2 μs long were used at 5 kHz repetition rate. It can be seen that the threshold current increases and the external differential quantum efficiency (η_d) decreases. For lasers on Si with various cavity lengths, the DLD densities observed by EL topography were the same at each

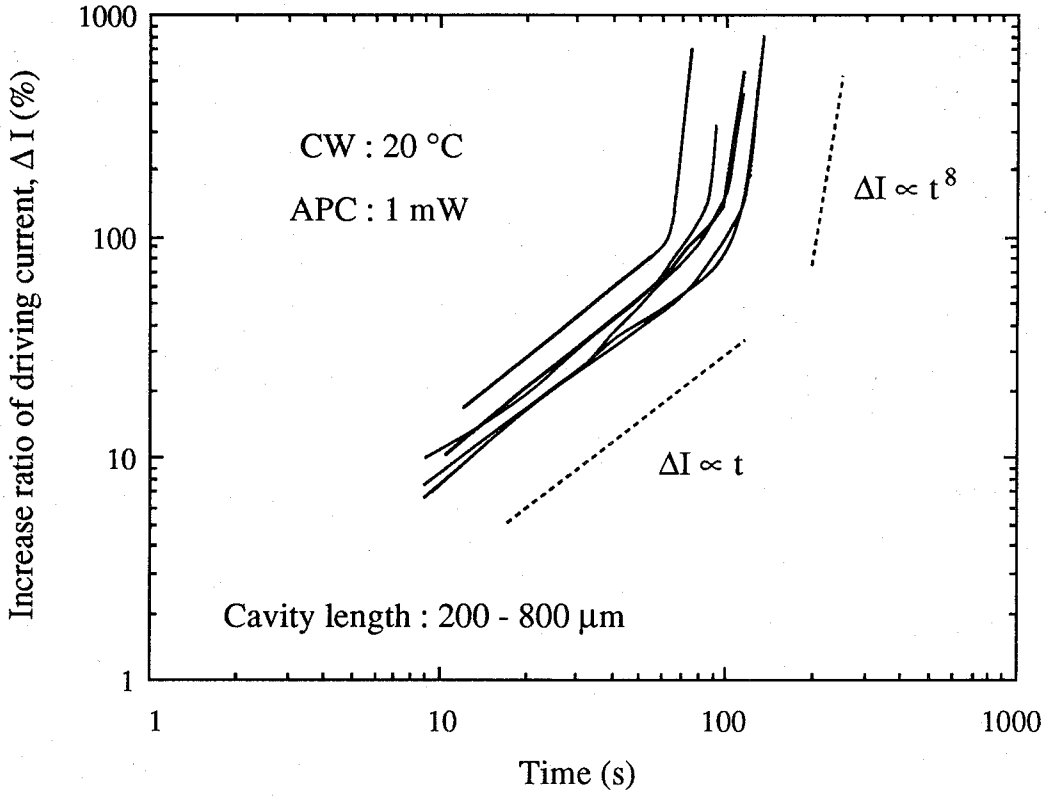

Fig. 2.2. Log-log relationship between increase ratio of driving current (ΔI) and aging time for AlGaAs/GaAs lasers on Si.

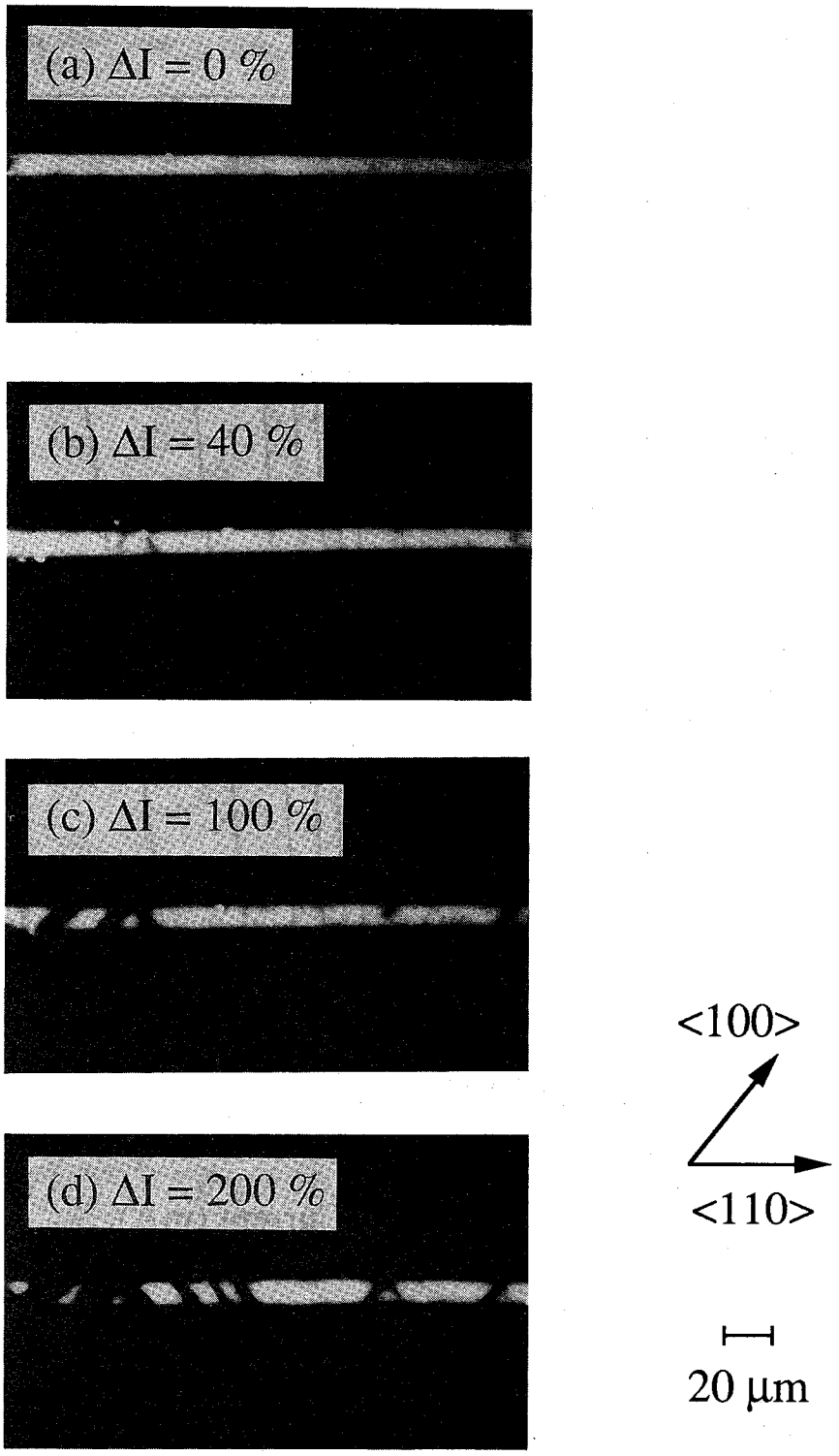

Fig. 2.3. Typical EL topographs of the laser on Si at each degradation stage of ΔI=(a) 0, (b) 40, (c) 100 and (d) 200 %.

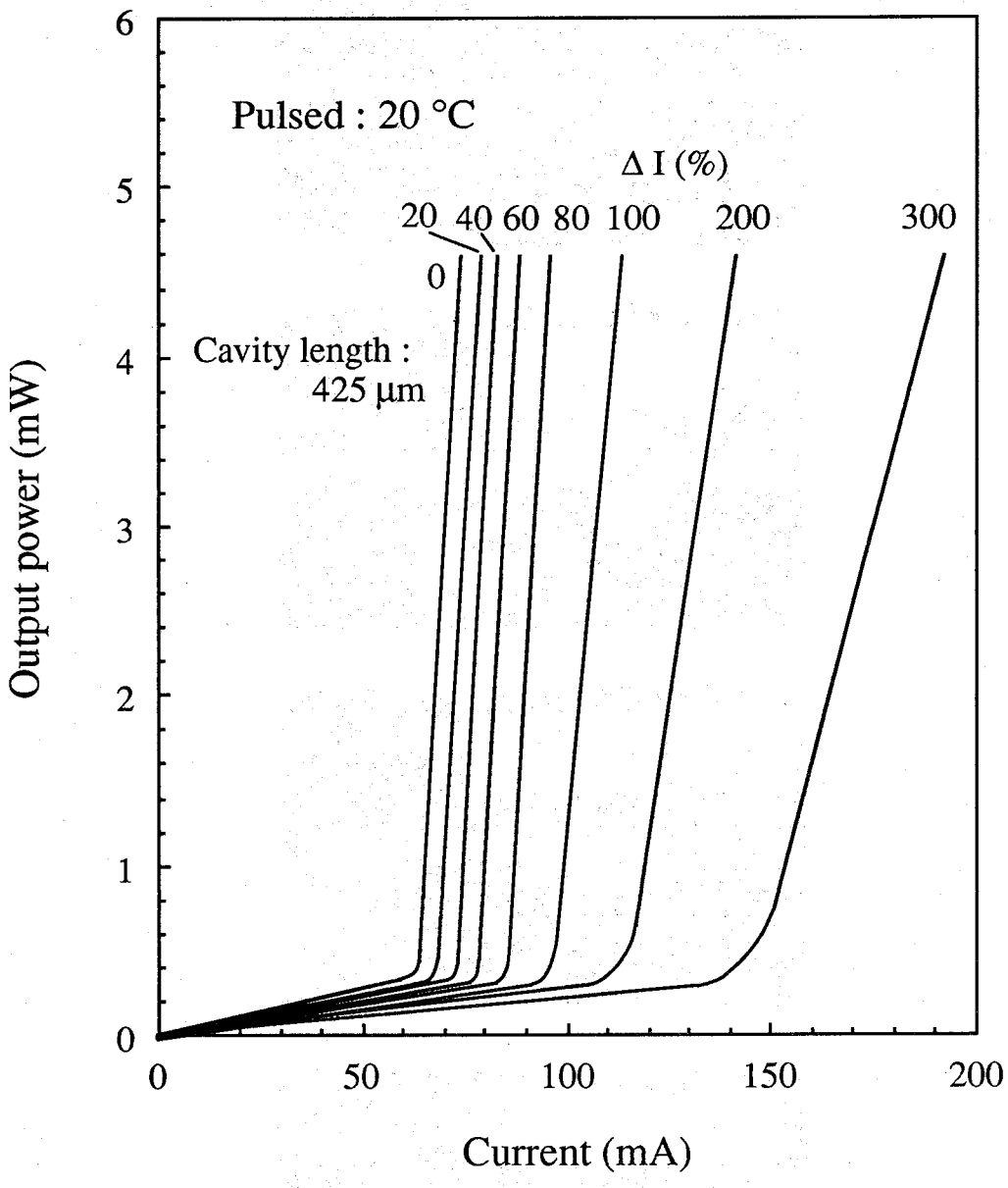

Fig. 2.4. Typical L-I characteristics of the laser on Si under pulsed condition at each degradation stage.

degradation stage. Therefore, the pulsed measurement was carried out for the lasers in order to estimate the change of the lasing characteristics. The lasing characteristic parameters such as η_i, α_i and β were determined using[9,10]

$$1/\eta_d = (1/\eta_i)\ [\ 1 + \alpha_i\ L/\ln(1/R)\ ], \qquad (2.2)$$

$$J_{th} = J_0/\eta_i + (\eta_i\beta\Gamma)^{-1}\ [\ \alpha_i + L^{-1}\ln(1/R)\ ], \qquad (2.3)$$

where L and R are cavity length and reflectivity of the mirror facet, respectively. The J_{th} is related to J_0 and Γ which are transparency current density and the optical confinement factor, respectively. Using the fact that the value of R is generally 0.32 for an uncoated facet, the values of η_i and α_i can be obtained from the relationship of $1/\eta_d$ versus L in eq. (2.2). This relationship at each degradation stage of ΔI = 0, 40, 100 % is shown in Fig. 2.5. It is found that η_i gradually decreases as the degree of degradation progresses. Assuming that Γ is 0.081 for the TQW laser[11], the values of b and J_0 can be estimated from eq. (2.3). Figure 2.6 shows the relationship of J_{th} versus $L^{-1}\ln(1/R)$ at each degradation stage. β is found to decrease gradually. Typical changes of lasing characteristics such as η_i, α_i and β, which are normalized by their initial values before degradation, are shown in Fig. 2.7. These initial values, $\eta_i(0)$, $\alpha_i(0)$ and $\beta(0)$, were 0.77, 25 cm^{-1} and 0.85 cm/A, respectively. At the initial slow degradation stage of ΔI < 60-80 %, η_i decreases markedly. The decrease in η_i seems to be caused by the increased number of nonradiative recombination centers. In order to study the increase of nonradiative recombination centers, the current-versus-voltage (I-V) characteristic of the laser on Si was measured at each degradation

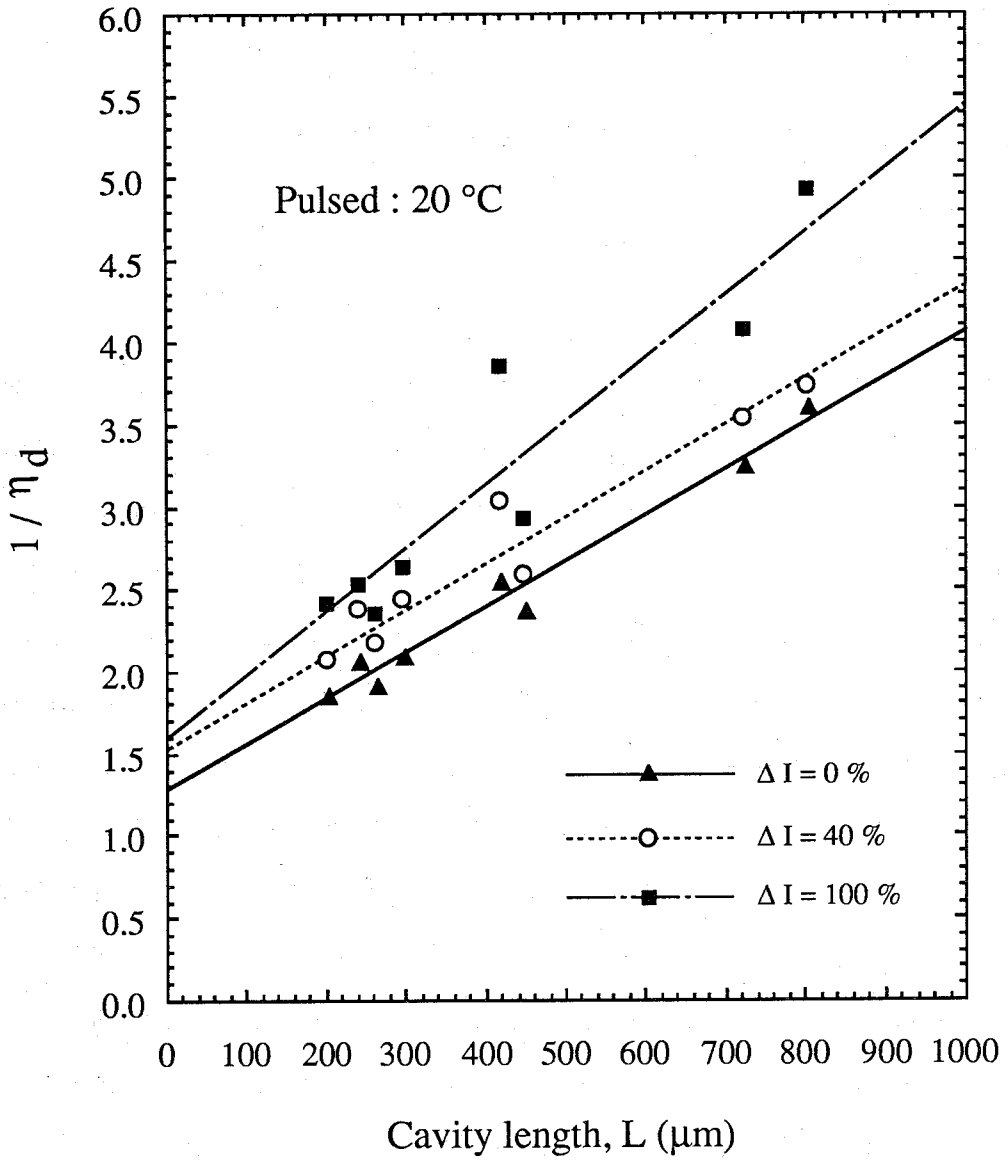

Fig. 2.5. Relationship of $1/\eta_d$ versus L for the laser on Si at each degradation stage.

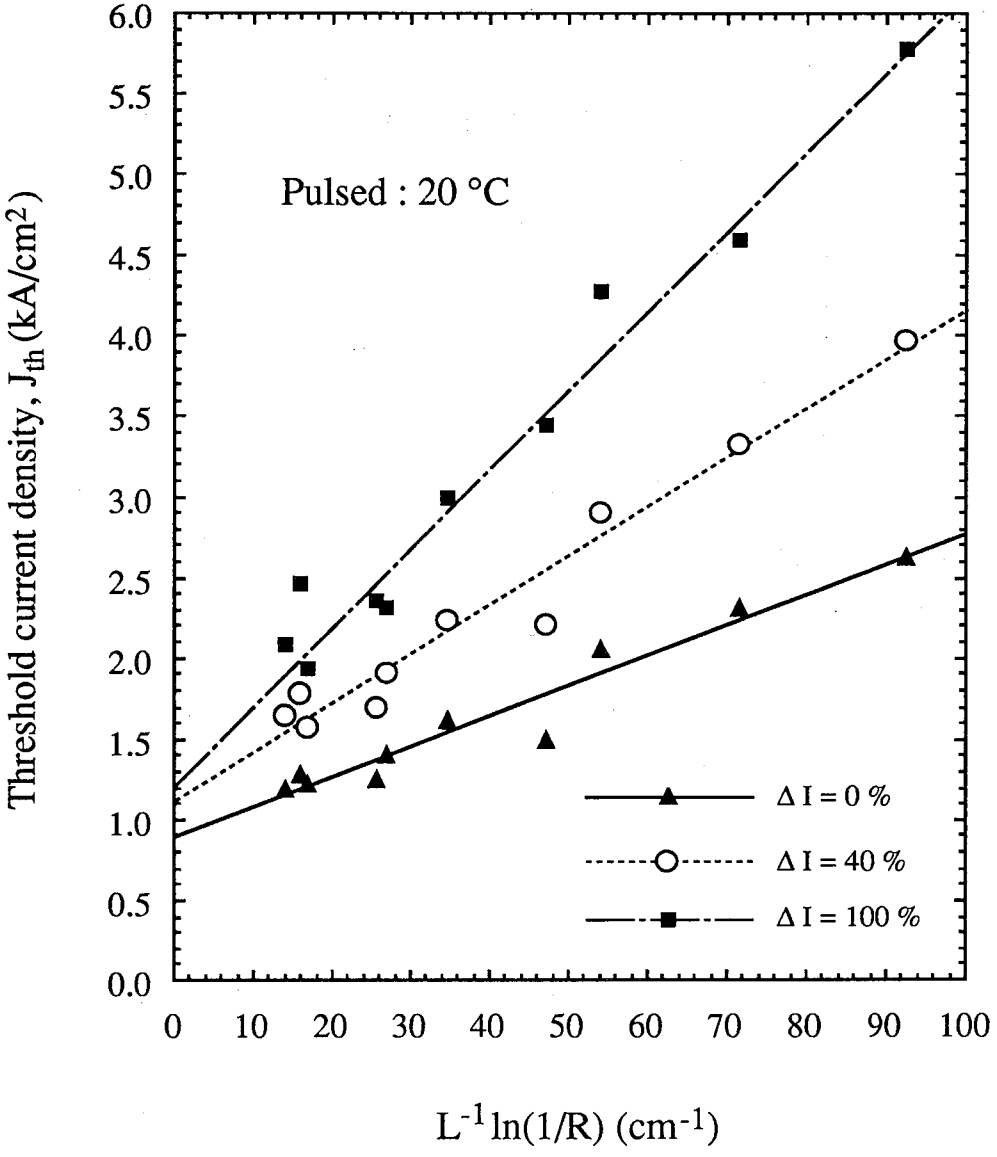

Fig. 2.6. Relationship of J_{th} versus $L^{-1}\ln(1/R)$ for the laser on Si at each degradation stage.

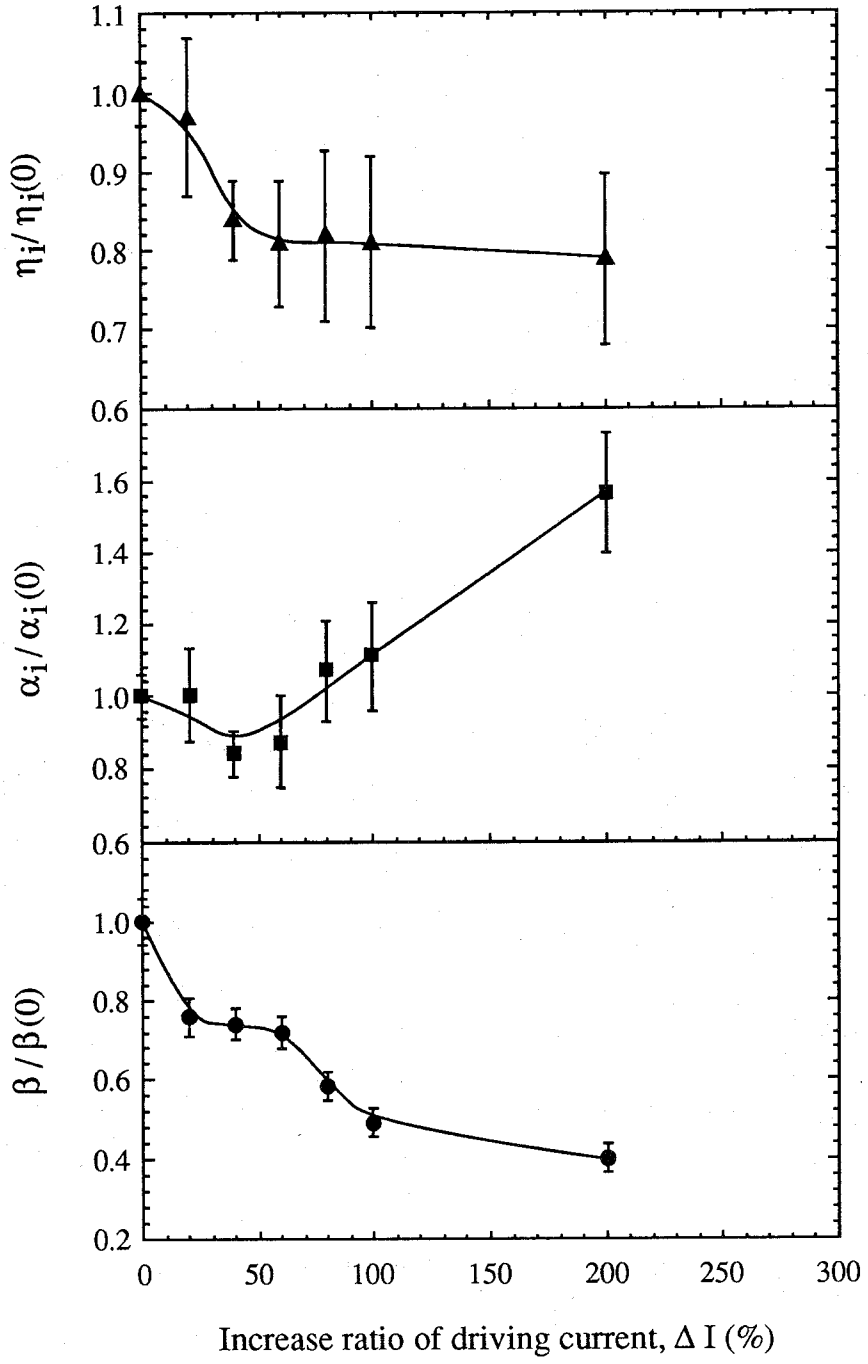

Fig. 2.7. Typical changes of $\eta_i/\eta_i(0)$, $\alpha_i/\alpha_i(0)$ and $\beta/\beta(0)$, normalized by initial values before degradation, as a function of increase ratio of driving current (ΔI) for the laser on Si.

stage. Figure 2.8 shows the typical change of recombination current (I_r) which has the ideality factor of 2. I_r was normalized by the initial value [$I_r(0)$] of 2.5 nA at 0.6 V, and the change of I_r was evaluated at this voltage. During the cw aging operation, the ideality factor was increased from 2.06 to 2.20. As shown in Fig. 2.8, I_r drastically increased at the initial slow degradation stage. Thus, the slow degradation related to the generation of <100> DLDs is probably caused by the increased nonradiative recombination current due to the increase of nonradiative recombination centers. Furthermore, the degradation is also caused by the decrease in β, as shown in Fig. 2.7. Although it can be seen that α_i slightly decreases at this degradation stage, the reason for this is not yet understood. At the subsequent rapid degradation stage of ΔI > 60-80 %, η_i negligibly changes, whereas α_i drastically increases and β markedly decreases. These results suggest that the rapid degradation due to the expansion of <100> DLDs is caused by increased absorption of emitted light and decreased gain.

2.4 Dependence of DLD Growth Velocity on Injected Current Density

2.4.1 <100> DLD Growth Velocity

It has been reported that the <100> DLD growth velocity for an AlGaAs/GaAs laser grown on the GaAs substrate generally depends on the injected current density[12]. The <100> DLDs are caused by the formation of complicated dislocation networks due to the recombination-enhanced dislocation climb (REDC) motion in the active region[13,14]. The injected carriers trapped by nonradiative recombination centers at DLDs emit the phonon energy which causes the lattice vibrations, resulting in enhancement of the REDC motion. For an AlGaAs/GaAs laser on Si, the dependence of the <100> DLD

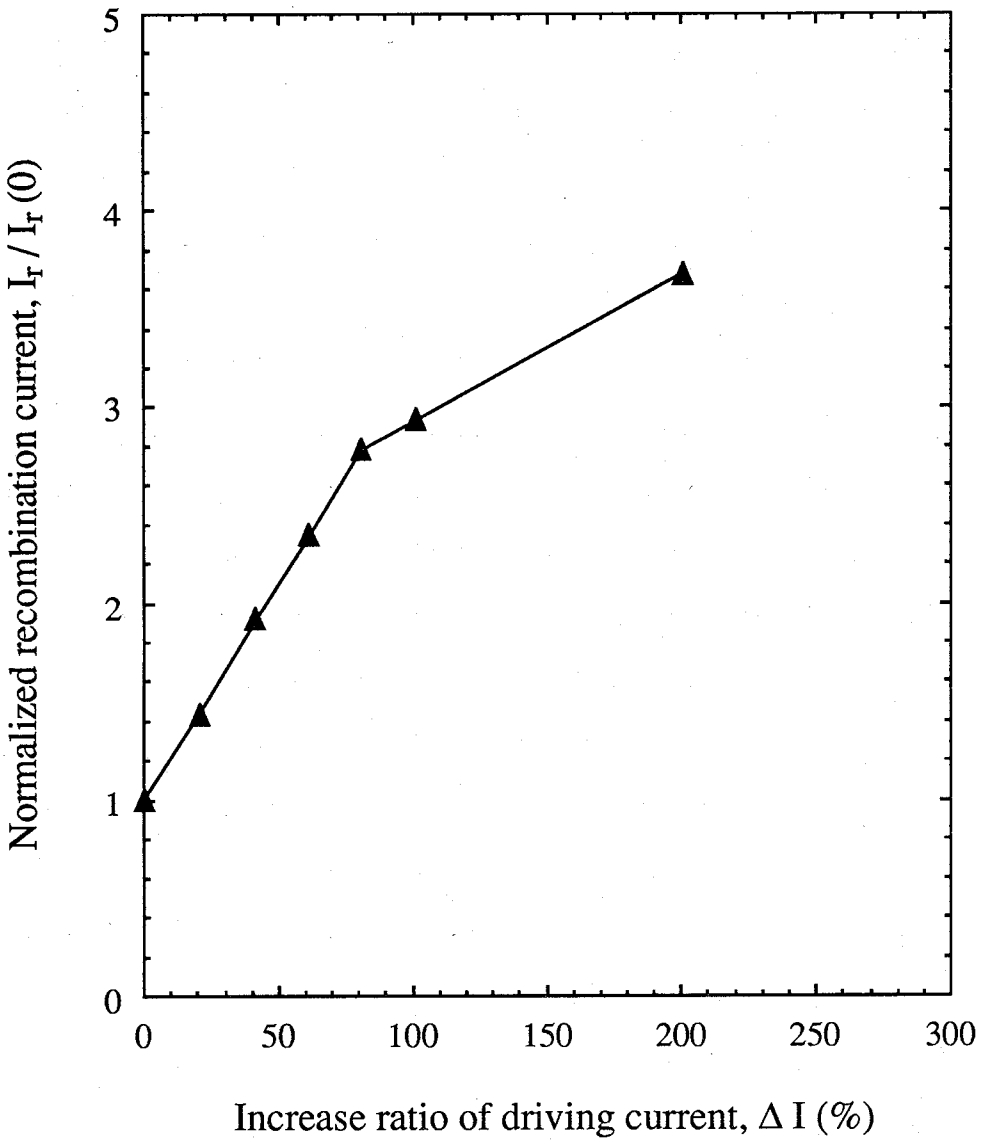

Fig. 2.8. Typical change of recombination current (I_r) as a function of increase ratio of driving current (ΔI) for the laser on Si.

growth velocity on the injected current density was studied for the first time. Figure 2.9 shows typical magnified EL topographs of an AlGaAs/GaAs TQW laser on Si under dc operation at a constant current density of 0.5 kA/cm^2 and temperature of 20 °C. No dark defects were observed before degradation [Fig. 2.9(a)]. At the first degradation stage [Fig. 2.9(b)], a few <100> DLDs were generated. In the subsequent stage [Fig. 2.9(c)], these DLDs extended toward the center of the active region.

Figure 2.10 shows the dependence of the <100> DLD growth velocity on the injected current density for an AlGaAs/GaAs TQW laser on Si at 20 °C. It can be seen that the DLD growth velocity strongly depends on the current density. The estimated DLD growth velocity was 14-25 μm/h at a current density of 1 kA/cm^2. On the other hand, it was reported that the <100> DLD growth velocity was estimated to be 2-10 μm/h at about 1 kA/cm^2 for an AlGaAs/GaAs SQW laser on GaAs[15]. The faster DLD growth velocity of the laser on Si is thought to be caused by the larger number of nonradiative recombination centers such as point defects in the active region than that of the laser on GaAs. It is known that the DLD growth is also enhanced by the rise of junction temperature of the laser[14,16]. The dependence of the <100> DLD growth velocity on the junction temperature was also studied for the laser on Si. The junction temperature is influenced by the injected current density and the ambient temperature under cw operation. The rise of junction temperature was estimated by measurement of the wavelength in the LED mode, because the wavelength shifts continuously by the rise of junction temperature. For example, the peak wavelength at 2.5 kA/cm^2 was about 5.4 nm longer than that at 0.5 kA/cm^2. Thus, it can be estimated that the junction temperature at 2.5 kA/cm^2 is about 30 °C higher than that at 0.5 kA/cm^2, because it is observed

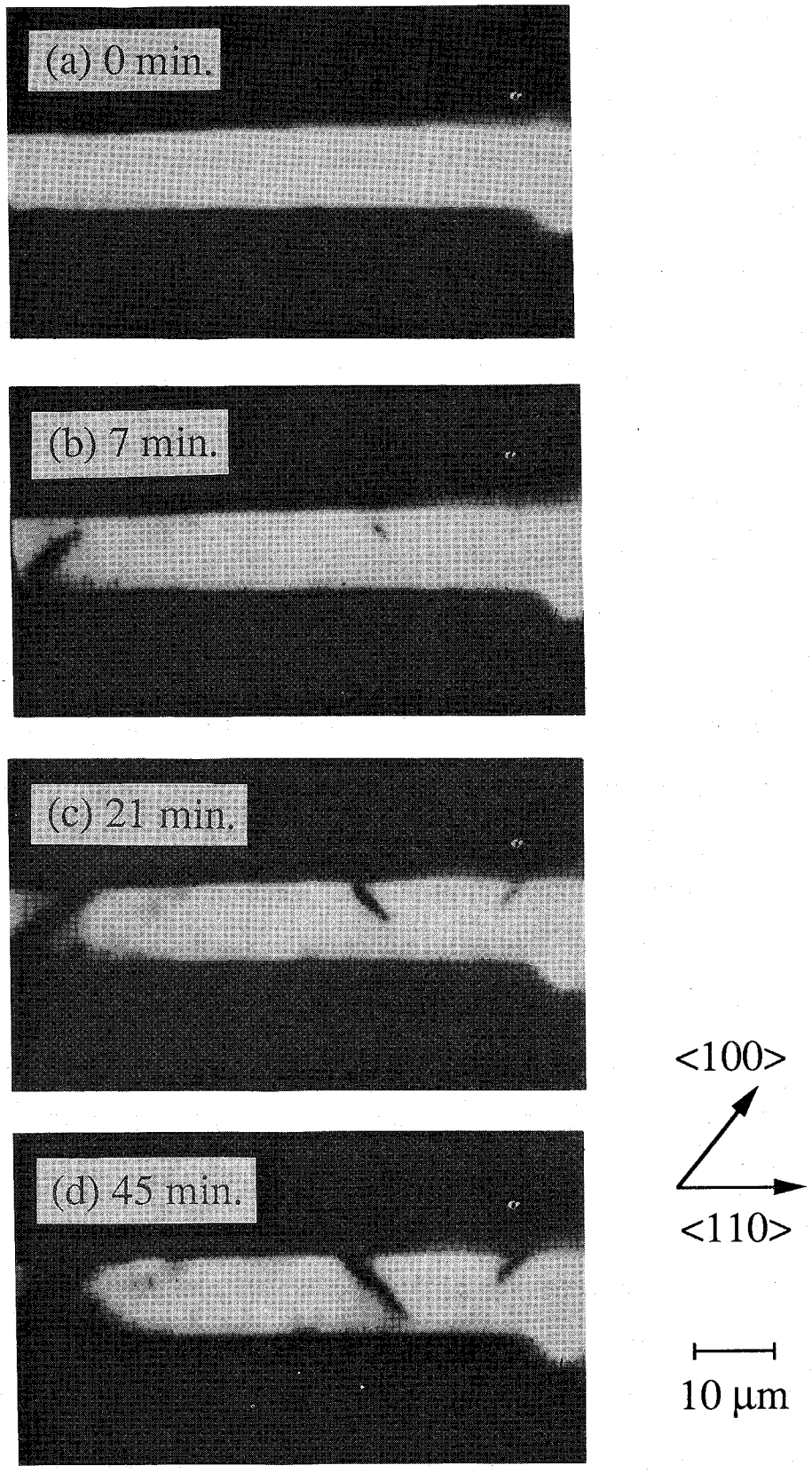

Fig. 2.9. Typical magnified EL topographs of the laser on Si after (a) 0, (b) 7, (c) 21 and (d) 45 min under dc operation at a constant current density of 0.5 kA/cm^2 and temperature of 20 °C.

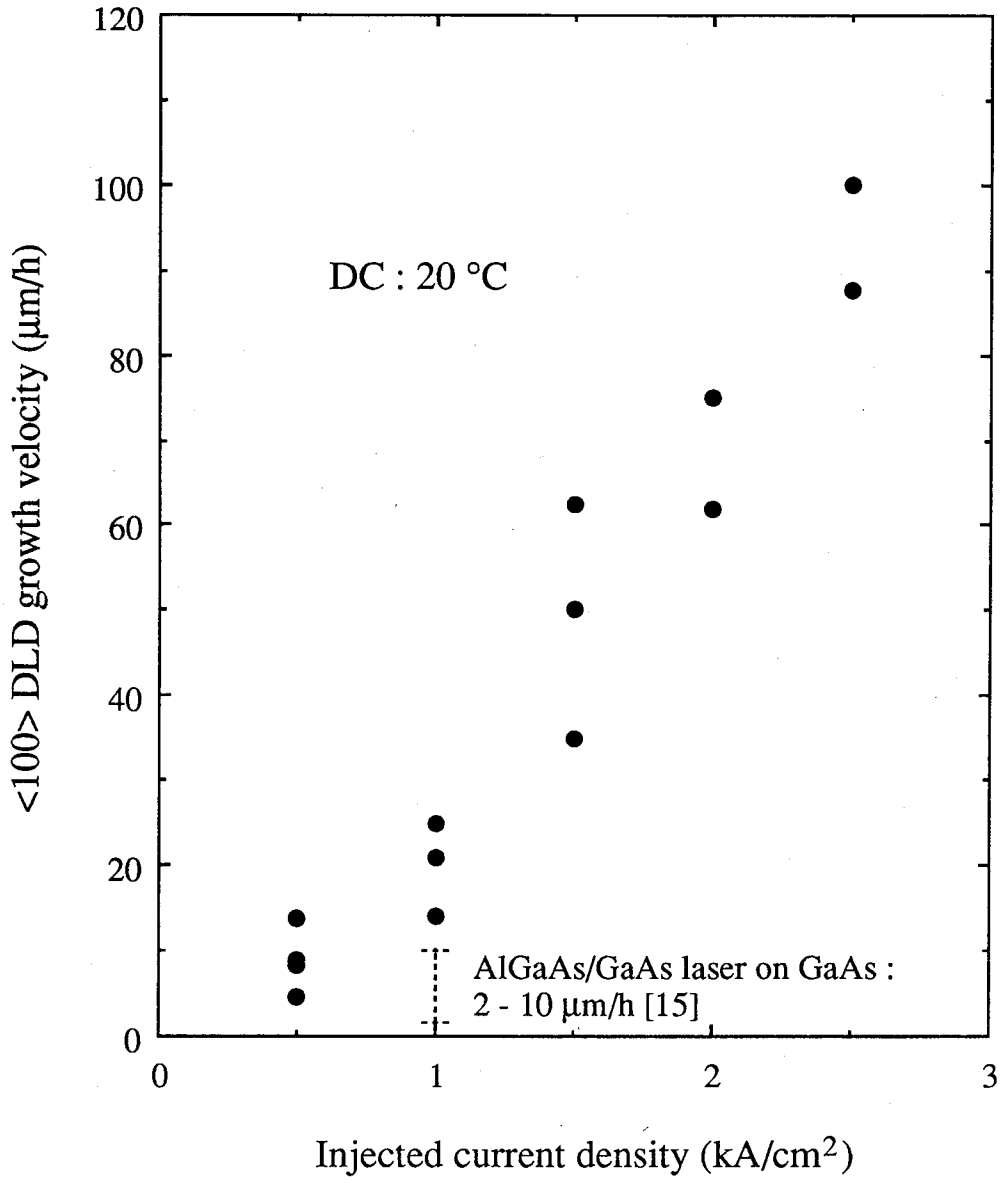

Fig. 2.10. Dependence of the <100> DLD growth velocity on the injected current density for the laser on Si at 20 °C.

that the wavelength of the laser on Si is shifted by about 0.18 nm/°C with variation in ambient temperature. For the current density of 0.5 kA/cm^2 at 50 °C, the DLD growth velocity was estimated to be 15-20 μm/h. This growth velocity is much slower than that of 2.5 kA/cm^2 at 20 °C. This result indicates that the DLD growth velocity depends more strongly on the injected current density than on the junction temperature. For suppressing the rapid degradation of the AlGaAs/GaAs laser on Si, the reduction of operating current density is very effective because this reduces the <100> DLD growth velocity.

2.4.2 <110> DLD Growth Velocity

The <100> DLDs have effective width in the <110> direction, and thus are regarded as <110> DLDs[12]. The cause of <110> DLDs is thought to be the growth of dislocations due to the recombination-enhanced dislocation glide (REDG) motion[14,17]. Matsui et al.[18] have also demonstrated that the <100> DLD was propagated by a combination of REDC and REDG motions. Therefore, the <110> DLDs in this study is thought to be caused by the REDG motion. The <110> DLDs for an AlGaAs/GaAs laser on GaAs are often observed by introducing high stress (~10^9 dyn/cm^2)[17]. Figure 2.11 shows the dependence of the <110> DLD growth velocity on the injected current density for an AlGaAs/GaAs TQW laser on Si at 20 °C. This estimated DLD growth velocity was 5-8 μm/h at a current density of 1 kA/cm^2. For the laser on Si, the <110> DLD growth velocity was estimated to be about 1/3 of the <100> DLD growth velocity. In contrast, it was reported that the <110> DLD growth velocity was about 1/10 of the <100> DLD growth velocity for an AlGaAs/GaAs laser on GaAs in the absence of high stress[12]. It appears that the faster <110> DLD growth velocity for the laser on Si is caused by its much higher

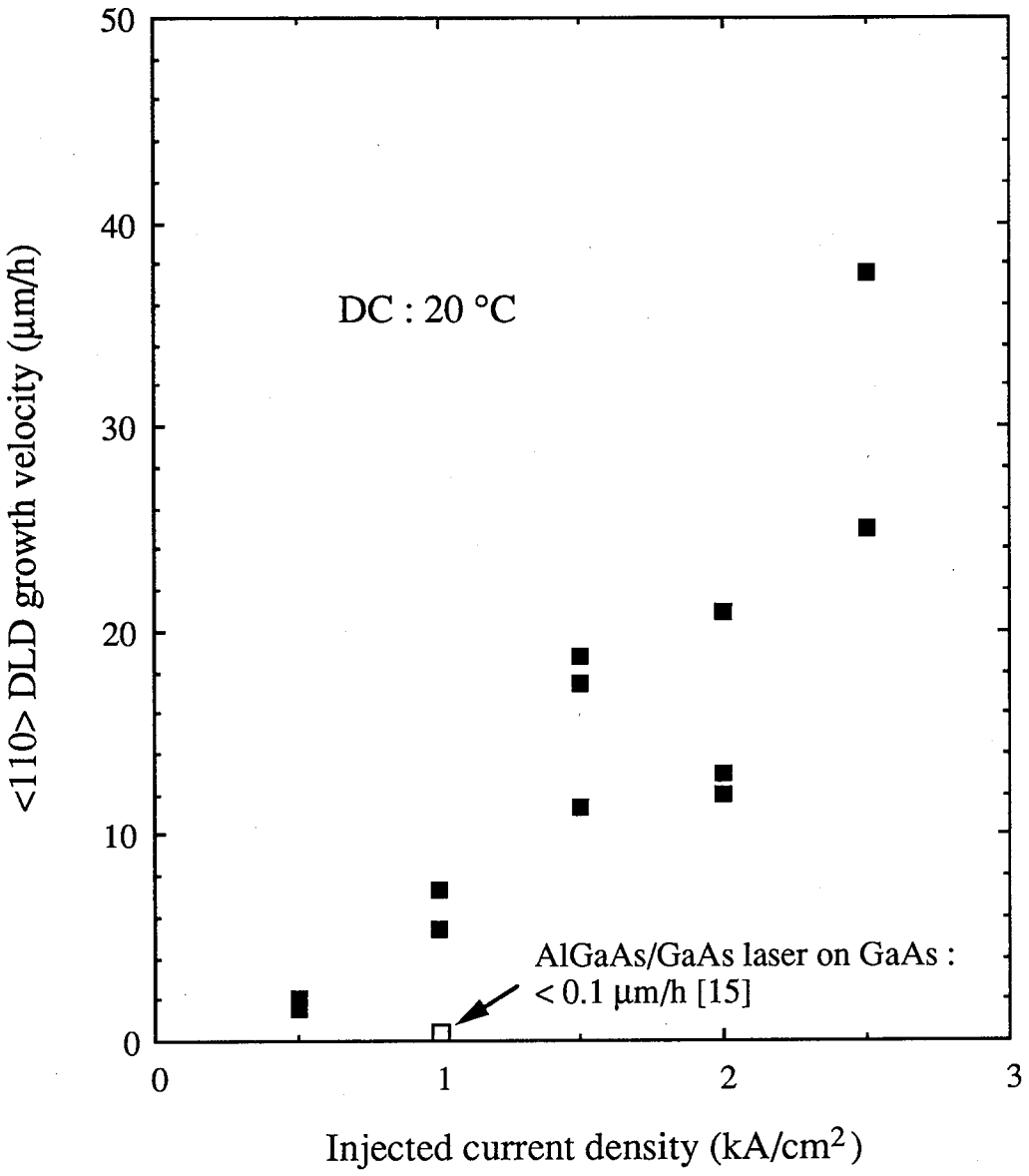

Fig. 2.11. Dependence of the <110> DLD growth velocity on the injected current density for the laser on Si at 20 °C.

residual tensile stress than that of the laser on GaAs.

Finally, a rapid degradation mechanism related to increased internal loss (absorption loss) due to both <100> and <110> DLDs is considered for an AlGaAs/GaAs laser on Si, as shown in Fig. 2.12. The <100> DLD is represented as an effective absorption region with effective width W_a and effective absorption coefficient α_{dl}[19]. For an AlGaAs/GaAs laser on GaAs with W_a of ~5 μm and α_{dl} of ~200 cm^{-1}, it was reported that the degradation due to the increase of α_i was mainly caused by the increase in the number of <100> DLDs (N_{dl})[19]. In contrast, the rapid degradation related to the increase of α_i for an AlGaAs/GaAs laser on Si seems to be caused by the increase of both N_{dl} and W_a. The increase of W_a is probably caused by the growth of <110> DLDs which result from the high residual stress for the laser on Si. The reduction of this stress seems to be also very important for the improvement of reliability of the laser on Si.

2.5 Conclusions

The influences of DLDs on lasing characteristics and the dependence of the DLD growth velocity on the injected current density for an AlGaAs/GaAs quantum well laser on Si have been studied. The generation of <100> DLDs caused the decrease of η_i and the slow increase of driving current. At the subsequent rapid degradation stage, expansion of the DLDs caused the remarkable increase of α_i and the decrease of β, and finally resulted in rapid increase of driving current. Furthermore, it was also found that the <100> and <110> DLDs growth velocities strongly depended on the injected current density. The <100> DLDs seem to have been caused by the formation of complicated dislocation networks due to the REDC motion in the vicinity of the threading dislocations in the active

<Top-viewed EL topograph>

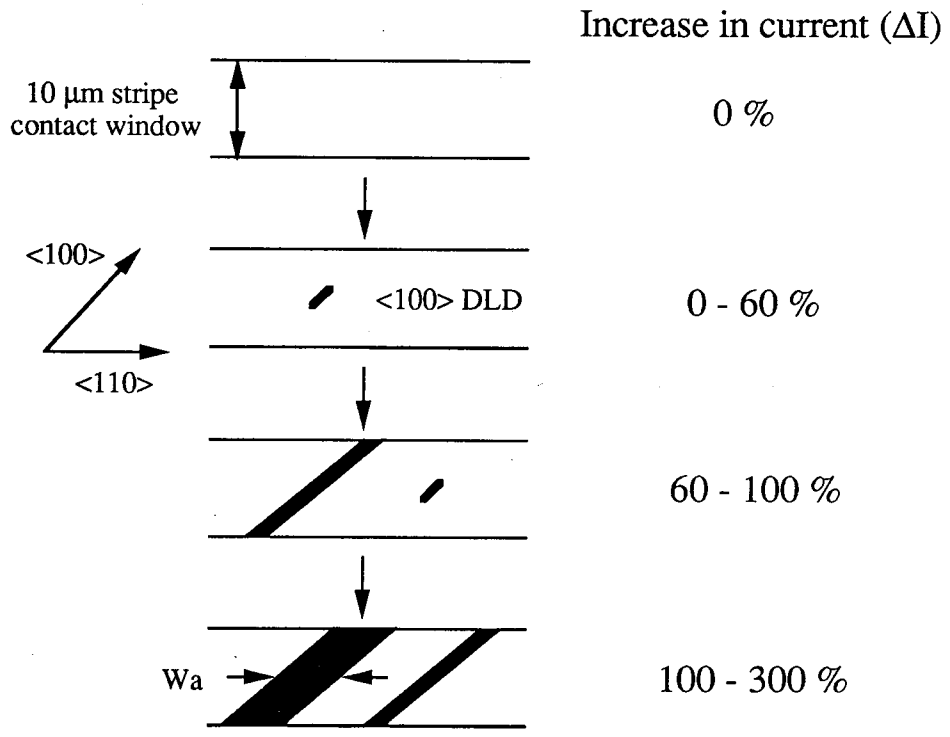

<Increasing internal loss>

$$\text{※}\quad \alpha_{id} = \alpha_{dl}\left(\frac{Ndl\ Wa}{L}\right) + \alpha_i(0)\left(\frac{L - Ndl\ Wa}{L}\right)$$

α_{id} : internal loss after degradation
$\alpha_i(0)$: internal loss before degradation
α_{dl} : effective absorption coefficient of <100> DLD
Ndl : number of <100> DLD
Wa : effective width of <100> DLD
L : cavity length

$$\alpha_{dl} \approx 200\ cm^{-1}\ ,\quad \alpha_i(0) = 25\ cm^{-1}$$

AlGaAs/GaAs laser on GaAs ; Ndl ↑ , Wa → ⇒ α_{id} ↗

AlGaAs/GaAs laser on Si ; Ndl ↑ , Wa ↑ ⇒ α_{id} ↑

Fig. 2.12. Rapid degradation mechanism related to increased internal loss for the laser on Si.

region. On the other hand, the <110> DLDs are thought to have originated from the growth of dislocations due to the REDG motion by the large residual thermal stress.

References

1) J. P. van der Ziel, R. D. Dupuis, R. A. Logan and C. J. Pinzone, Appl. Phys. Lett., **51**, 89 (1987).

2) J. P. van der Ziel and N. Chand, J. Appl. Phys., **68**, 2731 (1990).

3) R. B. Martins, P. Henoc, B. Akamatsu, G. Bartenlian and M. N. Charasse, J. Appl. Phys., **68**, 937 (1990).

4) T. Egawa, T. Jimbo, Y. Hasegawa and M. Umeno, Appl. Phys. Lett., **64**, 1401 (1994).

5) H. Okamoto, Y. Watanabe, Y. Kadota and Y. Ohmachi, Jpn. J. Appl. Phys., **26**, L1950 (1987).

6) T. Egawa, Y. Hasegawa, T. Jimbo and M. Umeno, Jpn. J. Appl. Phys., **31**, 791 (1992).

7) J. L. Merz and R. A. Logan, J. Appl. Phys., **47**, 3503 (1976).

8) Y. Hasegawa, T. Egawa, T. Jimbo and M. Umeno, Jpn. J. Appl. Phys., **34**, 2994 (1995).

9) H. Kressel and J. K. Butler: *Semiconductor Lasers and Heterojunction LEDs* (Academic, New York, 1977), p. 101.

10) W. T. Tsang, IEEE J. Quantum Electron., **QE-20**, 1119 (1984).

11) Y. Arakawa and A. Yariv, IEEE J. Quantum Electron., **QE-22**, 1887 (1986).

12) K. Fukagai, S. Ishikawa, K. Endo and T. Yuasa, Jpn. J. Appl. Phys., **30**, L371 (1991).

13) R. G. Waters, Prog. Quantum Electron., **15**, 153 (1991).

14) O. Ueda, J. Electrochem. Soc., **135**, 11C (1988).

15) R. G. Waters, D. P. Bour, S. L. Yellen and N. F. Ruggieri, IEEE Photon. Technol. Lett., **2**, 531 (1990).

16) M. Fukuda, K. Wakita and G. Iwane, J. Appl. Phys., **54**, 1246 (1983).

17) T. Kamejima, K. Ishida and J. Matsui, Jpn. J. Appl. Phys., **16**, 233 (1977).

18) J. Matsui, K. Ishida and Y. Nannichi, Jpn. J. Appl. Phys., **14**, 1555 (1975).

19) H. Yonezu, M. Ueno, T. Kamejima and I. Sakuma, Jpn. J. Appl. Phys., **13**, 835 (1974).